

# Time correlation functions and transport coefficients of two-dimensional Yukawa liquids

Z. Donkó<sup>1,2</sup>, J. Goree<sup>3</sup>, P. Hartmann<sup>1,2</sup>, Bin Liu<sup>3</sup>

<sup>1</sup>*Research Institute for Solid State Physics and  
Optics of the Hungarian Academy of Sciences,  
H-1525 Budapest, P.O. Box 49, Hungary*

<sup>2</sup>*Physics Department, Boston College,  
Chestnut Hill, MA 02467, USA and*

<sup>3</sup>*Department of Physics and Astronomy,  
The University of Iowa, Iowa City, Iowa 52242, USA*

(Dated: May 22, 2018)

## Abstract

The existence of coefficients for diffusion, viscosity and thermal conductivity is examined for two-dimensional (2D) liquids. Equilibrium molecular dynamics simulations are performed using a Yukawa potential, and the long-time behavior of autocorrelation functions is tested. Advances reported here as compared to previous 2D Yukawa liquid simulations include an assessment of the thermal conductivity, using a larger system size to allow meaningful examination of longer times, and development of improved analysis methods. We find that the transport coefficient exists for diffusion at high temperature, and viscosity at low temperature, but not in the opposite limits. The thermal conductivity coefficient does not appear to exist at high temperature. Further advances in computing power could improve these assessments by allowing even larger system sizes and longer time series.

PACS numbers: PACS: 52.27.Gr, 52.27.Lw, 82.70.-y

## I. INTRODUCTION

In strongly coupled dusty plasmas [1], consisting of micron-sized, highly charged particles, the interaction of the dust particles in many cases can be well approximated by the Yukawa potential. Other systems for which this type of potential is also appropriate include charged colloids [2] and high energy density matter [3].

The interparticle Yukawa potential energy in these systems,

$$\phi(r) = \frac{Q^2}{4\pi\epsilon_0} \frac{\exp(-r/\lambda_D)}{r}, \quad (1)$$

accounts for the Coulomb repulsion of the particles originating from their like charges ( $Q$ ) and the screening of the plasma which surrounds the dust particles. Screening is characterized by the dimensionless ratio  $\kappa = a/\lambda_D$ , where  $a$  is the Wigner-Seitz radius and  $\lambda_D$  is the screening length.

The coupling parameter  $\Gamma$  is a measure of interparticle potential energy as compared to kinetic energy. Defined as  $\Gamma = Q^2/(4\pi\epsilon_0 a k_B T)$ , it varies inversely with temperature  $T$ . In the strong-coupling domain  $\Gamma > 1$ , the system behaves like a non-ideal gas, liquid, and then solid, as  $\Gamma$  increases.

Dusty plasmas in nature and in laboratory environments appear in both three-dimensional (3D) and two-dimensional (2D) settings. A notable type of 2D systems is a layer of dust particles levitated in gaseous discharges. During the past decade this latter system has been investigated both experimentally and by different theoretical and simulation approaches. These studies at first mainly concerned the self-organized crystalline state of the system [4]. Propagation of compressional and shear waves has been studied and dispersion properties of these waves have been determined [5]. Using perturbation methods the generation of Mach cones and nonlinear waves has also been investigated [6]. Time scales in these 2D dusty plasma suspensions are characterized by  $\omega_0^{-1} = (Q^2/2\pi\epsilon_0 m a^3)^{-1/2}$ , where  $m$  is the dust particle mass.

These crystals can be melted, to produce an interesting liquid state, by changing the plasma parameters or by using laser heating techniques [7]. The strongly-coupled liquid state, established this way, has already attracted the interest in a series of experiments aimed at the observation of waves [8], as well as studies of transport processes [9]. Apart from experiments, combined theoretical and simulation studies have recently been carried

out in order to uncover thermodynamic and structural properties [10] as well as collective excitations [11] of two-dimensional Yukawa liquids. Studies of transport properties in such 2D systems are especially interesting due to the fact that doubts about the existence of transport coefficients in low dimensional systems have been raised on theoretical grounds [12, 13].

Experiments with dusty plasmas are invariably nonequilibrium problems, with a constant energy input and frictional energy loss. The energy input can be provided by ion flow or electric field fluctuations that propagate into the dust suspension from an outside source, or by external manipulation using for example laser radiation pressure. A major source of friction is gas drag experienced by the solid dust particles as they move through ambient neutral gas. At steady-state, the temperature is determined by a balance of the energy input and dissipation.

Molecular dynamics simulations have successfully been used for the determination of the self-diffusion [14], the shear viscosity [15, 16, 17, 18, 19] and the thermal conductivity [17, 20] coefficients of 3D Yukawa liquids.

In general, valid transport coefficients are more likely to exist in 3D liquids than in 2D. Here we will investigate 2D liquids. The first question to address is not how large a transport coefficient is, but rather does it exist at all. Assessing the existence of diffusion, shear viscosity and thermal conductivity coefficients in 2D Yukawa systems is the aim of this paper.

Assessing the existence of a transport coefficient in 2D Yukawa liquids based on simulation data has until now sometimes relied on qualitative judgments and data that covered too short a time span. Here we will attempt to improve on both of those limitations. We will use a larger system size, allowing us to calculate autocorrelation functions that are meaningful over a longer time span. We will reduce the qualitative aspect of the judgment by introducing quantitative analysis methods making use of Student's t-statistics to conclude whether a correlation function decays faster than  $1/t$ . We will also implement other improvements in the fitting that is part of the analysis, first to avoid errors that were previously caused by including the initial decay portions of the autocorrelation function(s), and second to generate error values required for the Student's t-statistics. Our assessment in the end cannot be viewed as a final word on the existence of a transport coefficient, but rather as an improved estimate that could in the future be improved further, especially with greater

computational power to provide better signal-to-noise ratios and even longer time spans.

In Sec. II of the paper we introduce the autocorrelation functions to be studied and present their general properties, while Sec. III briefly discusses previous work. In Sections IV and V, respectively, we explain the simulation and data analysis methods. The results are presented in Sec. VI. Section VII gives the conclusions of our studies.

## II. AUTOCORRELATION FUNCTIONS

For equilibrium systems, without gradients, transport coefficients are calculated using the Green-Kubo relations. For the three transport coefficients of interest here, these are given as follows [21].

For the diffusion coefficient,  $D$ ,

$$D = \frac{1}{N_d} \int_0^\infty C_v(t) dt, \quad C_v(t) \equiv \langle \mathbf{v}(t) \cdot \mathbf{v}(0) \rangle. \quad (2)$$

The integrand  $C_v(t)$  is the velocity autocorrelation function (VACF).

For shear viscosity,  $\eta$ ,

$$\eta = \frac{1}{VkT} \int_0^\infty C_\eta(t) dt, \quad C_\eta(t) \equiv \langle P_{ij}(t) P_{ij}(0) \rangle, \quad (3)$$

where the integrand  $C_\eta(t)$  is the shear stress autocorrelation function (SACF).

For thermal conductivity  $\lambda$ ,

$$\lambda = \frac{1}{VkT^2} \int_0^\infty C_\lambda(t) dt, \quad C_\lambda(t) \equiv \langle J_{Qi}(t) J_{Qi}(0) \rangle, \quad (4)$$

where the integrand  $C_\lambda(t)$  is the energy current autocorrelation function (EACF).

Here,  $N_d$  is the dimensionality of the system,  $V$  is the system volume,  $i \neq j$  are space coordinates, and the brackets  $\langle \rangle$  denote an ensemble average. Calculating the correlation functions requires time series data for the particle velocity  $\mathbf{v}$ , the off-diagonal element of the pressure tensor  $P_{ij}$ , and the energy current  $J_{Qi}$ ; these time series can all be recorded during a molecular dynamics simulation.

For transport coefficients to exist, the autocorrelation functions in the integrands of Eqs. (2)-(4) must decay rapidly enough for the integral to converge. This rapid decay for convergence is the essential requirement that we test in this paper. In examining their decay, it is crucial to examine the *long-time* behavior. Since the Green-Kubo integrals in Eqs. (2)-(4) extend in principle to infinity, what is really needed is information about the integrands

as  $t \rightarrow \infty$ . However, a numerical simulation is of course limited to a finite time span. This is one reason that a conclusion regarding the existence of a transport coefficient cannot be definitive when based on a simulation. Advances in computational power over the years will allow longer time spans, so that conclusions regarding the existence of a transport coefficient can change. Here we take a step in this gradual improvement by using a bigger simulation size, which allows a longer time span.

For the purpose of illustrating the autocorrelation functions, we present some examples in Fig. 1. Curves are shown for  $C_v$ ,  $C_\lambda$ , and  $C_\eta$ , all computed for a cool liquid ( $\Gamma = 300$  and  $\kappa = 2$ ). (Fig. 1 actually shows  $|C_v|$ , as this function may acquire negative values even at “early” times due to caged motion of particles.) We plot the data on log-log axes so that a power law behavior appears as a straight line.

Examining  $C_v$  in Fig. 1, we identify three portions of the time series. Our analysis will include only the central one of these three portions.

First, there are *initial decaying oscillations* in the correlation function. These are associated with caged particle motion, and are not of interest for diffusion.

In the middle, there is a portion we term *smooth decay*. This portion of the correlation function is what we seek to analyze, by examining and fitting it to determine whether it decays faster than  $1/t$ .

Finally, the smooth decay ends one of two ways: either a *sound peak* as seen in Fig. 1 for  $C_v$  and  $C_\lambda$ , or *noise oscillations with a zero crossing* as seen here for  $C_\eta$ . The sound peak occurs at a time that is the ratio of the length of the simulation box divided by the sound speed. Correlation data after the sound peak can be meaningless, especially in a solid or a cold liquid, because of the periodic boundary conditions, which mean that a sound wave that exits the box will re-enter the box from the other side. At long times, when the correlation function has diminished to a small value, it is obscured by noise, which can appear as oscillations crossing zero. We will not analyze data after a sound peak, or a zero crossing, whichever comes first.

### III. PREVIOUS WORK

In the study of liquids, long-time tails of autocorrelation functions have been the focus of numerous investigations. These have included both 3D and 2D systems, with various

interparticle potentials.

Non-exponential long-time tails in the VACF of *hard sphere and hard disk* systems were first reported by Alder and Wainwright [12]. For the 2D case they observed a  $\propto t^{-1}$  decay of the tail of the VACF, which makes the VACF non-integrable. As a consequence, the diffusion coefficient was claimed not to exist for this system.

Further, Ernst *et al.* [13] have shown that the *kinetic contributions* to the autocorrelation functions of shear stress and energy current – which are related to velocity correlations – exhibit the same behavior. Their findings were also confirmed by the calculations of Dorfman and Cohen [22]. Regarding systems with continuous potentials, power law decay of the VACF was observed in 3D soft-repulsive and Lennard-Jones liquids [23]. A  $t^{-1}$  tail of the SACF was found in molecular dynamics simulations in the case of 2D soft disk fluid [24]. For the case of Coulomb interaction (2D classical electron liquid) the existence of self-diffusion coefficient has been a topic of controversy [25, 26, 27].

For thermal conductivity, the present authors are aware of experiments but no previous simulation or theory for a strictly 2D (monolayer) Yukawa liquid. A recent experimental measurement of the thermal conductivity was reported for a 2D liquid in [28], following earlier measurements in 2D crystals [29] and liquids in a quasi-2D system [30].

The situation for self-diffusion and shear viscosity in 2D Yukawa liquids is different, as the literature includes both experimental and simulation studies. These have yielded estimates of the self-diffusion coefficient [31, 32] and the shear viscosity [9, 33, 34, 35]. Thus, our goals here will include reporting, apparently for the first time, a simulation for thermal conductivity in 2D Yukawa liquids, as well as an improvement over previous simulations for diffusion and viscosity.

For diffusion, earlier equilibrium MD simulations of 2D Yukawa liquids, restricted to  $\kappa = 0.56$ , predicted that superdiffusion rather than diffusion occurs over a wide range of temperatures [32]. They also predicted that  $D$  exists in the nonideal gas phase and near the disordering transition [40], and that the Stokes-Einstein relation  $D\eta \propto kT$  is violated very near the disordering transition.

Recent simulations [35] motivated by an experiment on the shear viscosity in 2D Yukawa liquids using a dusty plasma monolayer [9] indicated a fast decay of the SACF that allowed a calculation of a viscosity coefficient. Non-equilibrium simulations of the same system [36] did not show significant sensitivity of the results on system size and allowed an identification

of non-Newtonian behavior under high shear rates.

Interest in systems characterized by soft potentials motivates our investigations of 2D Yukawa liquids. Our aim is to carry out a systematic study of the time correlation functions and to investigate the existence of the related transport coefficients of 2D Yukawa liquids, covering a wide range of the  $\Gamma$  and  $\kappa$  parameters. Such investigations are especially timely now as very recent large-scale simulations of Isobe of a 2D hard disk fluid systems [37] have demonstrated that for some conditions the VACF decays *slightly but definitely* faster than  $1/t$ , in contradiction with the early findings of Alder and Wainwright [12] mentioned above.

Besides analyzing the correlation functions we also check the limits of applicability of the simulations, which has been missed in some previous studies.

## IV. SIMULATION TECHNIQUE

### A. Molecular dynamics method

It is noted that while nonequilibrium methods are generally more efficient in studies of transport phenomena, equilibrium simulations have the advantage of allowing a direct test for the existence of transport coefficients, as explained above. In cases when this test indicates that a valid transport coefficient does not exist, nonequilibrium simulations yield “transport coefficients” that may not be unique, in a way that they exhibit dependence on system size.

The system studied here is strictly two-dimensional, and it is under equilibrium conditions unlike some experiments, which are driven-dissipative [9]. Using this assumption we integrate the Newtonian equation of motion of the particles during the course of the simulation. We apply a rectangular cell with edge lengths  $L_x \cong L_y$ , and periodic boundary conditions. Pairwise Yukawa interparticle forces are summed over a  $\kappa$ -dependent cutoff radius (also extending into the images of the primary computational cell), using the chaining mesh technique. No thermostat is used, the desired system temperature is set by rescaling the momenta of the particles in the initialization phase of the simulation that precedes the start of data collection.

## B. Calculation of functions

The main results of the simulations are the correlation functions  $C_v(t)$ ,  $C_\eta(t)$ , and  $C_\lambda(t)$ , defined by Eqs. (2)-(4). In addition to these correlation functions, to detect diffusion we also calculate time series for the mean squared displacement of particles

$$\text{MSD}(t) = \langle |\mathbf{r}(t) - \mathbf{r}(0)|^2 \rangle. \quad (5)$$

The MSD has an advantage, as compared to the VACF, at high  $\Gamma$  where oscillations in the VACF obscure its decay. Diffusive motion is characterized by a constant time derivative of the MSD.

Phase space coordinates of the particles allow the determination of the VACF and MSD directly, while the time series needed to calculate the SACF and EACF are obtained from the phase space coordinates as [21]:

$$P_{xy} = \sum_{i=1}^N \left[ m v_{ix} v_{iy} - \frac{1}{2} \sum_{j \neq i}^N \frac{x_{ij} y_{ij}}{r_{ij}} \frac{\partial \phi(r_{ij})}{\partial r_{ij}} \right], \quad (6)$$

$$J_{Qx} = \sum_{i=1}^N v_{ix} \left[ \frac{1}{2} m |\mathbf{v}_i|^2 + \frac{1}{2} \sum_{j \neq i}^N \phi(r_{ij}) \right] - \frac{1}{2} \sum_{i=1}^N \sum_{j \neq i}^N (\mathbf{r}_i \cdot \mathbf{v}_i) \frac{\partial \phi(r_{ij})}{\partial r_{ij}}, \quad (7)$$

where  $\mathbf{r}_{ij} = \mathbf{r}_i - \mathbf{r}_j = (x_{ij}, y_{ij})$ . We normalize distances by the 2D Wigner-Seitz radius  $a = (1/n\pi)^{1/2}$ , where  $n$  is the areal density.

The first term on the right hand side of Eq.(6) is called the kinetic term, while the second term is the potential term, i.e.

$$P_{xy} = P_{xy}^{\text{kin}} + P_{xy}^{\text{pot}}. \quad (8)$$

Similarly, the energy current may be written as

$$J_{Qx} = J_{Qx}^{\text{kin}} + J_{Qx}^{\text{pot}} + J_{Qx}^{\text{coll}}, \quad (9)$$

where the three (kinetic, potential, and collision [38] or virial [39]) terms correspond to the ones on the right hand side of Eq.(7). (It is noted that some authors follow a different partitioning of the energy current.) The stress autocorrelation function (SACF) thus has the form

$$C_\eta = \langle P_{xy}^{\text{kin}}(t) P_{xy}^{\text{kin}}(0) \rangle + \langle P_{xy}^{\text{pot}}(t) P_{xy}^{\text{pot}}(0) \rangle +$$



$$2\langle P_{xy}^{\text{kin}}(t)P_{xy}^{\text{pot}}(0)\rangle = C_{\eta}^{\text{KK}} + C_{\eta}^{\text{PP}} + 2C_{\eta}^{\text{KP}}. \quad (10)$$

The energy current autocorrelation function (EACF) may as well be decomposed as

$$\begin{aligned} C_{\lambda} &= \langle J_{Qx}^{\text{kin}}(t)J_{Qx}^{\text{kin}}(0)\rangle + \langle J_{Qx}^{\text{pot}}(t)J_{Qx}^{\text{pot}}(0)\rangle + \\ &\quad \langle J_{Qx}^{\text{coll}}(t)J_{Qx}^{\text{coll}}(0)\rangle + 2\langle J_{Qx}^{\text{kin}}(t)J_{Qx}^{\text{pot}}(0)\rangle + \\ &\quad 2\langle J_{Qx}^{\text{kin}}(t)J_{Qx}^{\text{coll}}(0)\rangle + 2\langle J_{Qx}^{\text{pot}}(t)J_{Qx}^{\text{coll}}(0)\rangle = \\ &C_{\lambda}^{\text{KK}} + C_{\lambda}^{\text{PP}} + C_{\lambda}^{\text{CC}} + 2C_{\lambda}^{\text{KP}} + 2C_{\lambda}^{\text{KC}} + 2C_{\lambda}^{\text{PC}}. \end{aligned} \quad (11)$$

In calculating these correlation functions from simulation data, we use a common method of overlapping time segments. Each overlapping time segment begins at a different initial time in the time series. We average the correlation functions over all the overlapping segments. This averaging serves the role of an ensemble average. It also serves to reduce the noise.

For the VACF, we are also able to average over all the particles in the system, and this greatly reduces the noise as compared to the SACF and EACF, which allow only averaging over the overlapping segments. For this reason, noise presents a greater challenge for the SACF and EACF than for the VACF.

We repeat all the simulations several times (the actual numbers will be given for the cases presented later), each with different initial conditions for the particle positions. We combine the results of these runs, yielding a mean value and an error bar for each data point in the time series for the autocorrelation function.

## V. DATA ANALYSIS METHOD

Here we define in detail our analysis methods for the long-time behavior of the three autocorrelation functions. Our goal is to assess whether the functions decay faster than  $1/t$ , so that their integrals will converge and the corresponding transport coefficient exists. This assessment has in the past relied to a great extent on qualitative inspections of the autocorrelation functions. The analysis methods described below include improvements to invoke more quantitative criteria for this assessment. In the end we will answer the question of whether the transport coefficient exists along with a measure of our confidence in the conclusion.

### A. Fitting the correlation function

First, we choose the time range for our analysis. This is done by inspecting a plot of the correlation function  $C(t)$  on log-log scales, as in Fig. 1. We select a starting time and a stopping time.

The starting time will be selected usually as a judgment of the time when the initial decay ends. This judgment is qualitative, which is a concern because we are attempting to reduce the role of qualitative judgments. Therefore, we will bracket this time and produce our final results for two or three different starting times, to judge whether the slightly arbitrary choice of a starting time has much impact. In some cases, instead of a qualitative judgment of the initial decay, we will use a crossover of the separate terms contributing to the SACF or EACF to determine the starting time. We believe that in some previous simulations [35], a starting time was chosen too soon, so that the analysis included a great deal of the initial decay, so that the results should not be relied upon. It is only because we now use a larger simulation size, so that the sound peak occurs later, that we can detect that this problem occurred in previous simulations of a smaller size.

The stopping time will be the sound peak or a zero crossing, whichever comes first. In the example of Fig. 1, the analysis will stop at the sound peak for the VACF and EACF, but at a zero crossing for the SACF. To detect how sensitive our result is to the stopping time, we repeat all our calculations using 95% of the zero crossing as stopping time.

Second, we fit the data between the starting and stopping times to a power-law decay,

$$\log[C(t)] = \alpha \log(t) + \text{intercept}. \quad (12)$$

To avoid introducing a bias by overemphasizing data at long times, before fitting we resample  $C(t)$  at times that are uniformly spaced when plotted with a logarithmic axis.

Our fit to Eq. (12) uses a calculation of a  $\chi^2$  surface. The surface is calculated in the parameter space of the slope  $\alpha$  and the intercept. This method requires error bars for each data point in  $C(t)$ . We produce these error bars by performing multiple simulations for the same conditions but different initial conditions, and calculating the mean and standard deviation of the mean for each data point in  $C(t)$ .

An example of a  $\chi^2$  surface is shown in Fig. 2. The best fit is the minimum of the  $\chi^2$  surface, yielding  $\alpha_{\text{fit}}$ . The quality of the fit is evaluated by comparing the minimum  $\chi^2$  to

1.00, which is considered a typical value for a moderately good fit. In order to perform further statistical analysis we require an uncertainty, or standard error, for the fit parameter  $\alpha$ . We estimate this uncertainty  $\sigma_\alpha$  using the 68.3% confidence interval in the  $\chi^2$  surface, as shown in Fig. 2.

## B. Hypothesis testing

To complete our analysis, we use Student's t-statistics to compare  $\alpha_{\text{fit}}$  to  $-1$ . First, we compose a null hypothesis

$$H_0 : \alpha_{\text{fit}} > -1. \tag{13}$$

In other words, our null hypothesis  $H_0$  is that the transport is anomalous. We calculate the  $t$  value as

$$t = \frac{\alpha_{\text{fit}} + 1}{\sigma_\alpha}. \tag{14}$$

Next, we calculate the  $p$ -value for a one-tailed test using a Student's t-calculator. The  $p$ -value is the probability of  $\alpha > -1$ . Finally, we determine a significance level,  $1 - p$ , to reject  $H_0$ . Thus, in the end we determine the significance level for a conclusion that the transport is anomalous.

To explain this in physical terms, we are attempting to reject the null hypothesis that the transport coefficient does not exist, i.e., to reject the idea that the transport is anomalous. If we find that the significance level for this test is very high, for example 99%, we would be confident in saying that the transport coefficient exists. However, if the significance level is much lower, for example 60%, we would be unable to conclude whether the transport coefficient exists. As always with Student's t-statistics, the test of the null hypothesis works only one way. We contemplate whether we can reject  $H_0$ , not the converse. Thus, if we find a small  $p$ -value such as 0.05 we will conclude that the transport is not anomalous, with a significance level  $1 - p$ . If we instead find a large  $p$ -value such as 0.40, the test does not yield a quantitative conclusion but we can examine the correlation function graph qualitatively for indications that suggest the transport is anomalous.

## VI. RESULTS AND DISCUSSION

Most of the correlation function data presented below are based on several independent simulation runs, each with  $1.1 \times 10^6$  time steps (typically spanning a time several times  $10^4 \omega_0^{-1}$ ), carried out on systems of  $N = 4080$  or  $16\,320$  particles. After preparing the correlation functions, when we use the  $\chi^2$  surface method, we limit the analysis to two cases. These are a cool liquid with  $\Gamma = 300$  and a warm liquid with  $\Gamma = 20$ , both for  $\kappa = 2$ . These cases correspond to temperatures of  $1.4 T_M$  and  $21 T_M$ , respectively, using data for the melting point  $T_M$  from [10]. Results for the  $\chi^2$  surface and Student's t-method are presented in Tables I-IV.

### A. VACF and Diffusion

To diagnose diffusive motion, we present the analysis of the velocity autocorrelation functions (VACF) in Figs. 3–5 for a range of  $\Gamma$  and  $\kappa$  values.

#### 1. VACF

We will investigate the decay of the VACF curves plotted in Fig. 3 for  $\kappa = 2$ . These data represent the average of 6 simulation runs (for each  $\Gamma$ ) using  $N = 4080$  particles. The curves have the three portions described earlier. In the middle there is a smooth decay, which will be our primary focus. This is preceded by initial decaying oscillations associated with caged motion, and it is followed by a sound peak (marked  $S$ ) and noisy oscillations. Plotting the data on log-log axes reveals a power law, when the smooth decay appears to be a straight line. For reference, we draw a line with a slope of  $-1$ , corresponding to a  $t^{-1}$  decay. Diffusion, as opposed to anomalous diffusion, would require a decay faster than  $t^{-1}$  so that the integral of the VACF converges.

Our statistical analysis using the  $\chi^2$  method is presented in Table I. Two cases are listed here. For a warm liquid,  $\Gamma = 20$ , we find that the fit parameter for the slope is typically  $\alpha \approx 1.20$ , depending slightly on the starting and stopping times used in selecting the data to fit. Performing the Student's t-analysis leads to the conclusion that we can reject the null hypothesis  $H_0$  of anomalous transport with an 83 – 99% significance level. The fits with the best  $\chi_{\min}^2$  have a 99% significance level. Thus, our simulation indicates that the diffusion

coefficient exists for this warm liquid. On the other hand, for a cold liquid,  $\Gamma = 300$ ,  $\alpha$  is very near to one, and we cannot reject the null hypothesis  $H_0$  of anomalous transport.

To further illustrate this trend of diffusive motion, we present in Fig. 4(a) fitting results for a range of  $\Gamma$ . (For ease in performing repeated calculations, here we found  $\alpha$  using a simpler fitting method with only a single set of starting and stopping times, so that the results are less precise than in Table I and do not have error bars or significance levels.) Results are reported here for three values of  $\kappa$ , which all have different melting points. To better compare these, we rescaled the horizontal axis as  $T/T_M$  in Fig. 4(b), using data for the melting point  $T_M$  from [10]. After performing this rescaling, we find a nearly universal curve: near the melting point or disordering transition at  $T/T_M = 1$  there is anomalous diffusion, while at higher temperatures the motion is likely to be diffusive. A transition between the regimes of diffusive and anomalous particle transport appears at  $T/T_M \approx 5$ .

## 2. System size effects

Next we analyze the possible effects related to the finite size of the computational box. These effects are illustrated here for the VACF, but the limitations we find are also applicable to the other correlation functions, the SACF and the EACF.

The finite size of the simulation box limits usefulness of simulation data in two different ways. First, particles may traverse a small simulation box without experiencing a sufficient number of collisions. This may be a concern only for low  $\Gamma$  values. Second, sound waves have a finite transit time  $\Delta t_s$  across the box [23] as was already mentioned above. Due to the periodic boundary conditions, this can limit meaningful interpretation of correlation functions to  $t < \Delta t_s$ . This is a concern especially at high  $\Gamma$ , where correlations of caged particle motion [41], which appear as oscillations in the correlation function, persist a long time. For our purposes we wish to interpret correlation functions after these oscillations have decayed; at high  $\Gamma$  this requires a long time series and thus a large system size. The peaks marked  $S$  in Fig. 3 and are conspicuous indications of this effect.

Random particle motion can be decomposed into a spectrum of sound waves over a range of wavenumbers. The sound waves have a dispersion, where the group velocity depends on wavenumber, but this dispersion is significant only for large wavenumbers [11]. For small wavenumbers the wave has little dispersion, so that there is a distinctive sound speed.

This sound speed depends on the shielding parameter  $\kappa$ . For  $\kappa = 1, 2$ , and  $3$ , respectively, the sound speeds for such waves are  $c \cong 0.78 a\omega_0$ ,  $c \cong 0.4 a\omega_0$ , and  $c \cong 0.22 a\omega_0$  [11]. The corresponding transit times are expected to be  $\omega_0\Delta t_s = \sqrt{N\pi}/c = 290, 560$ , and  $950$ , for  $\kappa = 1, 2$ , and  $3$ , respectively, for a simulation box with edge length  $L = a\sqrt{N\pi}$  and  $N = 16\ 320$  particles.

We see the effect of  $\kappa$  in Fig 5(a), where VACFs show a sound peak that reduces the useful portion of the data most extremely for small  $\kappa$ . (The values of the coupling parameter  $\Gamma$  have been varied among the three curves to keep constant the effective coupling value [10]  $\Gamma^* = 85$ .)

The effect of system size on the sound peak is demonstrated in Fig 5(b). Note that at the smallest system size ( $N = 1020$  particles) the part of the VACF with power law decay completely disappears. This shows that a large system size is essential, if one is to identify and fit the decay portion of the correlation function. This problem becomes more extreme for small  $\kappa$  values where the sound speed is higher [cf. Fig 5(a)]. For this reason, we believe that our results represent an advance over some earlier simulations with small system sizes, where the latter should no longer be relied upon.

Improving the transit time comes with a significant computational cost. As  $\Delta t_s$  scales as  $N^{1/2}$ , doubling the useful long-time range of the VACF requires quadrupling the runtime, because the number of computations in the simulation scales linearly with  $N$ .

### 3. MSD

As an additional test for diffusion, to gain confidence in our conclusions based on the VACF, we examine the long-time behavior of the mean-square displacement (MSD). This method makes use of the same kind of simulations, but we use only particle position data to calculate a time series of squared displacements from an initial position, and average this over all particles and overlapping time segments. To do this, we performed additional simulations with a larger system size of  $N = 16\ 320$  particles, but only with a single simulation run. The MSD results are plotted in Fig. 6. First we emphasize that due to the sound speed, the useful long-time range of the MSD curves is the same as that for the VACFs. Around the time of  $\Delta t_s$ , marked  $S$ , ripples show up on the MSD curves (with an amplitude that is detectable, but too small to see in Fig. 6 without more magnification. These ripples hinder

the determination of the slope at longer times. Thus any analysis of the MSD curves must be limited to times not exceeding  $\Delta t_s$ .

The MSD time series plotted in Fig. 6(a) indicate a ballistic motion at low  $\omega_0 t$  values, characterized by  $\text{MSD} \propto t^2$ . At later times the slope of the MSD curves decays, and for  $\omega_0 t \gtrsim 100$  most of the curves appear to be nearly linear,  $\langle(\Delta r)^2\rangle \propto t^\gamma$  with slopes  $\gamma \gtrsim 1$ .

As a more sensitive indicator, we examine the derivative  $\text{MSD}'$  of the MSD in Fig. 6(b). This derivative would have a zero slope, at long time, if motion is diffusive. Instead, we find *superdiffusion*, as indicated by an exponent  $\gamma \approx 1.15$ , over the range of  $\Gamma \geq 100$  where the  $\text{MSD}'$  curves have a constant slope. At  $\Gamma < 100$  the slopes of the  $\text{MSD}'$  curves change slightly but continuously in the time domain extending to  $\Delta t_s$  [indicated by dotted vertical lines in Fig. 6(a) and (b)]. We speculate that the decreasing slope of the  $\text{MSD}'$  at lower  $\Gamma$  values may eventually, beyond the meaningful time range shown here, converge to zero, which is required for normal diffusion. We can, however, not prove this speculation, as several orders of magnitude longer time may be needed to reach this convergence. A more convincing demonstration of convergence of the MSD might require as much as three orders of magnitude additional  $\Delta t_s$ , which would require  $\sim 10^{10}$  particles, far beyond our computing capacity. Nevertheless, the observation of a decreasing slope  $\text{MSD}'$  curves at lower  $\Gamma$  values is generally consistent with the findings that the VACFs decay faster than  $t^{-1}$  at these (lower)  $\Gamma$  values [cf Fig. 3(a)], also indicating normal diffusion.

## B. SACF and Shear viscosity

Turning now our attention to the shear viscosity, we present the stress autocorrelation functions in Fig. 7. Two cases are shown: a warm liquid at  $\Gamma = 20$ , and a cool liquid at 300, both at  $\kappa = 2$ . These data are for a large system size of  $N = 16\,320$ , with 108 and 115 independent simulation runs for  $\Gamma = 20$  and 300, respectively, each comprising  $1.1 \times 10^6$  time steps. It is noted that in the first part of calculations 52 and 31 runs have been carried out for  $\Gamma = 20$  and 300, respectively. The data obtained from these runs have been analyzed in the way explained in Sec. V A, and the results of this analysis are given in Table II. Having selected the most appropriate start and stop times, several additional independent simulation runs have subsequently been carried out (resulting a total number of runs of 108 and 115, for  $\Gamma = 20$  and 300, respectively) and the data analysis was accomplished only for

this pair of start and stop times. The best fits obtained here are also given in Table II. (The same procedure was followed for the EACF, to be discussed in the next subsection.)

For the warm liquid,  $\Gamma = 20$ , we observe a power-law tail with a decay slower than  $1/t$ . Fitting the decay using our  $\chi^2$  method yields small exponents in the range  $-0.63 > \alpha > -0.80$ , as listed in Table II. A Student's t-test yields  $p$ -values that do not allow rejecting the null hypothesis of anomalous transport. Examining the SACF graph in Fig. 7, we verify that the decay does appear to be slower than  $1/t$ . Thus, our simulation indicates that the viscosity coefficient does not exist for the warm liquid.

This result, that the shear viscosity does not exist for a 2D Yukawa liquid at a warm temperature, is contrary to what was previously believed. The difference in our result is presumably attributable to the larger simulation size, allowing us to observe the smooth decay after the initial decay.

For the cool liquid, with the higher coupling value of  $\Gamma = 300$ , we find the opposite result. A qualitative inspection of the total SACF in Fig. 7 shows a rapid decay, faster than a power law.

We can gain greater confidence in this conclusion for the cool liquid by examining the separate contributions to the SACF, in Fig. 8. These contributions are the potential (PP), kinetic (KK) and cross (KP) terms [as given by Eq. (10)]. Curves shown in Fig. 8 are again for  $\Gamma = 20$  and  $\Gamma = 300$ , at  $\kappa = 2$ . The values on the vertical axis have been normalized so that  $C_\eta(t = 0)$ , given as Eq.(10), equals 1.

For the cool liquid at  $\Gamma = 300$ , the potential term dominates at early times. More importantly, at longer times we see a useful indication that possibly has not been previously reported: the potential term begins to oscillate, so that it possibly does not dominate the long-time behavior. At these long times,  $\omega_0 t > 80$ , the kinetic term might instead dominate, and it decays as a power law. This observation leads us to fit only the kinetic term, and we find an exponent mostly in the range  $-1.29 > \alpha > -1.38$ , and we can reject the null hypothesis of anomalous viscosity with a significance level of 72 – 99%, as listed in Table III.

For the warm liquid at  $\Gamma = 20$ , the kinetic contribution to the shear viscosity dominates in Fig. 8, as is well known [16, 35]. In Fig. 8 we see that the potential term decays rapidly into the noise, so that only the kinetic term contributes significantly to the long-time tail. Because we see no crossover between the various terms at long time, we have greater confidence in our conclusion, based on the total SACF, that the SACF for the warm liquid decays slowly



and the viscosity coefficient does not exist.

### C. EACF and Thermal conduction

Finally we analyze the behavior of the energy autocorrelation functions (EACF). The EACF for  $\kappa = 2$  at  $\Gamma = 20$  and 300 are plotted in Fig. 9. These curves are the results of averaging the same numbers of runs as specified for the case of the SACF, using  $N = 16\ 320$  particles.

The initial decay persists for a long time in the EACF, as compared to the VACF [Fig. 3(a)] or the SACF at low  $\Gamma$  [Fig. 7(a)]. We judge the initial decay for the EACF in Fig. 9 to last until the a power law becomes apparent at  $\omega_0 t \approx 70$  in the case of  $\Gamma = 20$ , and  $\omega_0 t \approx 170$  in the case of  $\Gamma = 300$ . We will focus our attention now on the “smooth decay” that occurs after this initial decay, and before the first zero crossing.

For the warm liquid,  $\Gamma = 20$ , we see in Fig. 9 a slow power-law decay. As listed in Table IV, we find a power-law exponent in the range  $-1.16 > \alpha > -1.02$ , which is close to a  $t^{-1}$  decay. The  $p$ -values do not allow rejecting the null hypothesis of anomalous transport. Examining the curves qualitatively in Fig. 9, we conclude that the decay is likely too slow for convergence. Thus, our simulation indicates that in this warm liquid, the thermal conductivity coefficient does not exist.

For the cool liquid,  $\Gamma = 300$ , our results are hindered by a short and noisy “smooth decay” between the long initial decay and the oscillations with zero crossings. Fitting, we find in Table IV an exponent of  $\alpha = -1.40 \pm 0.87$ . The fit is not very reliable, as indicated by the wide error bar on this value, as well as a high value of  $\chi_{\min}^2$  in Table IV. We are thus unable to conclude whether the thermal conductivity exists for the cool liquid. Improving this result would require more extensive computations to improve the signal-to-noise ratio in the EACF at long times.

We now examine the separate contributions to the EACF in Fig. 10. For  $\Gamma = 20$ , there is an apparent crossover of the KK and CC terms. This crossover may coincide with the end of the rather long initial decay that we judged in the total EACF of Fig. 9. For  $\Gamma = 300$ , on the other hand, there is no crossover, giving us more confidence in our analysis above based on the total EACF.

Our results here for the EACF are apparently the first that have been reported for a

2D Yukawa liquid. We note that the EACF poses especially challenging computational requirements because the useful portion of the curve is at large  $t$  when the signal-to-noise ratio is poorest. Improving the signal-to-noise ratio for the EACF at  $\Gamma = 300$  to a level that would allow a conclusion would require at least an order of magnitude increase in runs beyond the 115 runs we used. We concluded that our simulation indicates the thermal conductivity coefficient does not exist for a warm liquid, but for a cool liquid, our signal-to-noise ratio did not allow a conclusion.

## VII. SUMMARY

It has long been suggested, for two-dimensional systems in general, that valid transport coefficients do not exist [13]. Here we reported some counter-examples, based on our calculations covering a wide range of parameters of 2D frictionless Yukawa liquids. We find that transport coefficients sometimes exist, depending on the temperature:

- The diffusion coefficient exists for warm but not for cool liquids. For warm liquids, the diffusion coefficient exists at temperatures higher than about five times the melting temperature. For cool liquids, however, we found a closely  $\propto t^{-1}$  type decay of the velocity autocorrelation function (VACF), indicating the occurrence of anomalous diffusion and no valid diffusion coefficient.
- The shear viscosity coefficient exists for cool but not warm liquids. This finding is contrary to previously reported results. For  $\kappa = 2$ , a cool liquid at  $\Gamma = 300$  exhibits a fast decay indicating a valid transport coefficient, but a warm liquid at  $\Gamma = 20$  does not. Comparing to the result above, our simulations suggest that self-diffusion and viscosity do not couple, because the coefficients do not exist in the same temperature regimes.
- The thermal conductivity, assessed here for the first time, does not exist for a warm liquid at  $\Gamma = 20$ , where a slow power-law decay in the energy autocorrelation function (EACF) was observed. For a cool liquid at  $\Gamma = 300$ , however, we are unable to come to a conclusion because of the technical challenges posed by signal-to-noise ratios and a long initial decay.

Our approach has been to ask the question, does the transport coefficient exist? Using equilibrium MD simulations, this question was addressed by computing autocorrelation functions, and examining their decay at long times. A rapid decay would indicate that the integral of the autocorrelation function converges, and the corresponding transport coefficient exists. For the results reported here, we have improved our statistical analysis methods for assessing whether the decay is faster than  $1/t$ , as required for convergence.

A limitation of equilibrium MD methodology is that testing for convergence requires reliable measurements of correlation functions at times tending to infinity, while the simulations yield results over only a finite time. This finite time is limited by two challenges: signal-to-noise ratios (which are especially important for the shear viscosity and thermal conductivity) and sound peaks arising from periodic boundary conditions (especially important for the diffusion coefficient). Both of these problems have been improved here by using larger simulation sizes than in previous reports. For this paper, we consumed several years of CPU time, using typical personal computers. Nevertheless, the simulation data did not allow us to draw definite conclusions regarding the existence of transport coefficients in cases when the decay of correlation functions was close to  $1/t$ .

Future advances in computational power will allow larger simulation sizes. The increase in size that is needed is substantial, because of the square-root scaling of the sound peak time with respect to system size  $N$ . A  $10^4$  fold increase in computations would be required for a 100-fold increase in meaningful time.

Because of these limitations that are gradually being offset by improved computing power, conclusions like those we presented above (i) should be considered as a snapshot view of a developing effort to estimate whether transport coefficients exist in 2D Yukawa liquids and (ii) may even change just like in the case of 2D hard disk system ([12] vs. [37]). Our results are, nevertheless, valuable because of interest in 2D liquids in general, and also because of increased interest in transport measurements in 2D dusty plasma experiments.

We can identify other areas where further work would be useful. Higher temperature liquids, in the non-ideal gas phase, have not been well explored yet. Systems present in 2D dusty plasma experiments – which include friction and particle heating [9], [29] – can be simulated by MD methods with proper modification of the particles' equation of motion. Another line of research could be the identification of the reasons behind the anomalous transport and its dependence on the dimensionality of the system. Such an investigation has

been presented in [42] for diffusion.

### Acknowledgments

This work was supported by the Hungarian Fund for Scientific Research and the Hungarian Academy of Sciences, OTKA-T-48389, OTKA-IN-69892, MTA-NSF-102, OTKA-PD-049991. J.G. and B. L. were supported by NASA and DOE.

- 
- [1] *Focus on Complex (Dusty) Plasmas* New J. Phys. **5** (2003); R. L. Merlino and J. Goree, *Physics Today*, **57**, 32 (2004).
  - [2] H. Löwen *et al.*, J. Phys. A **36**, 5827 (2003); S. Auer and D. Frenkel, J. Phys. Condens. Matter **14**, 7667 (2002).
  - [3] *Strongly Coupled Coulomb Systems*, Ed. by G. J. Kalman, K. B. Blagoev, and M. Rommel (Plenum Press, NY, 1998); M. S. Murillo, Phys. Plasmas **11**, 2964 (2004).
  - [4] H. Thomas, G. E. Morfill, V. Demmel, J. Goree, B. Feuerbacher, and D. Möhlmann, Phys. Rev. Lett. **73**, 652 (1994); A. Melzer, V. A. Schweigert, I. V. Schweigert, A. Homann, A. Peters, and A. Piel, Phys. Rev. E **54**, R46 (1996).
  - [5] S. Nunomura, D. Samsonov, and J. Goree, Phys. Rev. Lett. **84**, 5141 (2000).
  - [6] A. Melzer, S. Nunomura, D. Samsonov, Z.W. Ma, and J. Goree, Phys. Rev. E **62**, 4162 (2000).
  - [7] M. Wolter and A. Melzer, Phys. Rev. E **71**, 036414 (2005).
  - [8] S. Nunomura, S. Zhdanov, D. Samsonov, and G. Morfill, Phys. Rev. Lett. **94**, 045001 (2005); A. Piel, V. Nosenko, and J. Goree Phys. Plasmas **13**, 042104 (2006).
  - [9] V. Nosenko and J. Goree, Phys. Rev. Lett. **93**, 155004 (2004).
  - [10] P. Hartmann, G. J. Kalman, Z. Donkó, and K. Kutasi, Phys. Rev. E **72**, 026411 (2005); P. Hartmann, Z. Donkó, P. Bakshi, G. J. Kalman, and S. Kyrkos, IEEE Trans. Plasma Sci. **35**, 332 (2007).
  - [11] G. J. Kalman, P. Hartmann, Z. Donkó, and M. Rosenberg, Phys. Rev. Lett. **92**, 065001 (2004).
  - [12] B. J. Alder and T. E. Wainwright, Phys. Rev. A **1**, 18 (1970).
  - [13] M. H. Ernst, E. H. Hauge, and J. M. J. van Leeuwen, Phys. Rev. Lett. **25**, 1254 (1970).
  - [14] H. Ohta and S. Hamaguchi, Phys. Plasmas **7**, 4506 (2000).

- [15] K. Y. Sanbonmatsu and M. S. Murillo, Phys. Rev. Lett. **86**, 1215 (2001).
- [16] T. Saigo and S. Hamaguchi, Phys. Plasmas **9**, 1210 (2002).
- [17] G. Salin and J.-M. Caillol, Phys. Rev. Lett. **88**, 065002 (2002); G. Faussurier and M. S. Murillo, Phys. Rev. E **67**, 046404 (2003).
- [18] T. S. Ramazanov, K. N. Dzhumagulova, O. F. Petrov, and A. V. Gavrikov, Proc. of 33rd EPS Conference on Plasma Phys. Rome, 19 - 23 June 2006 ECA Vol. 30I, P-4.031 (2006).
- [19] Z. Donkó and P. Hartmann, Phys. Rev. E **78**, 026408 (2008).
- [20] Z. Donkó and P. Hartmann, Phys. Rev. E **69**, 016405 (2004).
- [21] J.-P. Hansen and I. R. McDonald, *Theory of simple liquids* (Academic Press, New York, 1976).
- [22] J. R. Dorfman and E. G. D. Cohen, Phys. Rev. A **6**, 776 (1972).
- [23] A. McDonough, S. P. Russo, and I. K. Snook, Phys. Rev. E **63**, 026109 (2001).
- [24] G. P. Morriss and D. J. Evans, Phys. Rev. A **32**, 2425 (1985).
- [25] J. P. Hansen, D. Levesque, and J. J. Weis, Phys. Rev. Lett. **43**, 979 (1979).
- [26] M. Baus and J. Bosse, Phys. Rev. A **22**, 2284 (1980).
- [27] G. K. Agarwal and K. N. Pathak, J. Phys. C: Solid State Phys. **16**, 1887 (1983).
- [28] V. Nosenko, S. Zhdanov, A. Ivlev, G. Morfill, J. Goree and A. Piel, Phys. Rev. E, **100**, 025003 (2008).
- [29] S. Nunomura, D. Samsonov, S. Zhdanov, and G. Morfill, Phys. Rev. Lett. **95**, 025003 (2005).
- [30] V. E. Fortov, O. S. Vaulina, O. F. Petrov, M. N. Vasiliev, A. V. Gavrikov, I. A. Shakova, N. A. Vorona, Yu. V. Khrustalyov, A. A. Manohin, and A. V. Chernyshev, Phys. Rev. E **75**, 026403 (2007).
- [31] S. Nunomura, D. Samsonov, S. Zhdanov, and G. Morfill, Phys. Rev. Lett. **96**, 015003 (2006).
- [32] Bin Liu and J. Goree, Phys. Rev. E **75**, 016405 (2007).
- [33] A. Gavrikov, I. Shakhova, A. Ivanov, O. Petrov, N. Vorona, and V. Fortov, Phys. Letters A **336**, 378 (2005).
- [34] O. S. Vaulina and I. E. Dranzhevski, Phys. Scripta **73**, 577 (2006).
- [35] Bin Liu and J. Goree, Phys. Rev. Lett. **94**, 185002 (2005).
- [36] Z. Donkó, J. Goree, P. Hartmann, and K. Kutasi, Phys. Rev. Lett. **96**, 145003 (2006).
- [37] M. Isobe, Phys. Rev. E **77**, 021201 (2008).
- [38] J. Eapen, J. Li, and S. Yip, Phys. Rev. Lett. **98**, 028302 (2007).
- [39] J. de Andrade and H. Stassen, J. Molecular Liquids **110**, 169 (2004).

- [40] Bin Liu, J. Goree, and O. S. Vaulina, Phys. Rev. Lett. **96**, 015005 (2006).
- [41] Z. Donkó, G. J. Kalman, and K. I. Golden, Phys. Rev. Lett. **88**, 225001 (2002); J. Daligault, Phys. Rev. Lett. **96**, 065003 (2006).
- [42] T. Ott, M. Bonitz, Z. Donkó, and P. Hartmann, Phys. Rev. E **78**, 026409 (2008).

TABLE I: Results for fitting the  $C_v$ , the velocity autocorrelation function (VACF). Various starting and stopping times, normalized by  $\omega_0$ , are tested. For the warm liquid,  $\Gamma = 20$ , the  $p$ -values are small, leading us to reject  $H_0$  with an 80 – 99% significance level and to conclude that the diffusion coefficient exists. For the cool liquid,  $\Gamma = 300$ , the  $p$ -values do not allow us to conclude anything.  $\kappa = 2$ .  $N_R$  is the number of runs included in the data analysis.

$\Gamma$	Stop	Start	$\alpha_{\text{fit}}$	$\sigma_\alpha$	$\chi_{\text{min}}^2$	$t$	$p$	$N_R$
20	190	20	-1.20	0.05	0.92	4.00	0.000	6
20	190	30	-1.22	0.09	0.20	2.59	0.005	6
20	190	45	-1.20	0.15	0.20	1.38	0.08	6
20	190	68	-1.17	0.20	0.20	0.85	0.20	6
20	180	20	-1.20	0.05	0.94	4.00	0.00	6
20	180	30	-1.22	0.09	0.20	2.44	0.01	6
20	180	45	-1.20	0.15	0.21	1.38	0.08	6
20	180	68	-1.19	0.20	0.21	0.95	0.17	6
300	236	100	-1.00	0.16	2.60	0.00	0.50	6
300	236	120	-1.05	0.44	0.54	0.11	0.45	6
300	236	148	-1.02	0.39	0.39	0.05	0.48	6
300	224	100	-1.00	0.16	2.70	0.00	0.50	6
300	224	120	-1.04	0.22	0.57	0.19	0.43	6
300	224	148	-1.02	0.41	0.41	0.05	0.48	6

TABLE II: Results for fitting the  $C_\eta$ , the stress autocorrelation function (SACF). Various starting and stopping times, normalized by  $\omega_0$ , are tested for the warm liquid,  $\Gamma = 20$ . The  $p$ -values are high, indicating that we cannot reject  $H_0$ .  $\kappa = 2$ .  $N_R$  is the number of runs included in the data analysis.

$\Gamma$	Stop	Start	$\alpha_{\text{fit}}$	$\sigma_\alpha$	$\chi_{\text{min}}^2$	$t$	$p$	$N_R$
20	120	30	-0.71	0.84	0.67	0.35	0.64	52
20	114	30	-0.67	0.82	0.69	0.40	0.66	52
20	120	20	-0.65	0.59	0.56	0.59	0.72	52
20	114	20	-0.63	0.70	0.57	0.53	0.70	52
20	120	13	-0.79	0.47	0.75	0.45	0.67	52
20	114	13	-0.80	0.52	0.76	0.39	0.65	52
20	120	20	-0.69	0.97	0.21	0.32	0.63	108

TABLE III: Results for fitting only the kinetic contribution to the stress autocorrelation function (SACF) for the cool liquid,  $\Gamma = 300$ . The  $p$ -values are small, so that we reject  $H_0$ .  $\kappa = 2$ .  $N_R$  is the number of runs included in the data analysis.

$\Gamma$	Stop	Start	$\alpha_{\text{fit}}$	$\sigma_\alpha$	$\chi_{\text{min}}^2$	$t$	$p$	$N_R$
300	300	20	-1.38	0.19	1.77	2.00	0.02	31
300	300	30	-1.36	0.31	0.91	1.16	0.12	31
300	300	45	-1.29	0.49	0.95	0.60	0.27	31
300	285	20	-1.38	0.19	1.79	2.05	0.02	31
300	285	30	-1.36	0.31	0.92	1.18	0.12	31
300	285	45	-1.29	0.49	0.96	0.59	0.28	31
300	300	45	-1.60	0.74	0.21	0.81	0.21	115



TABLE IV: Results for fitting the energy current autocorrelation function (EACF). Compared to the VACF and SACF, for the EACF we used fewer combinations of start and stop times due to the limited time duration between them. For  $\Gamma = 300$ , due to noise and a limited useful time range, the fit quality as indicated by  $\chi_{\min}^2$  is not good, and we cannot rely strongly on the corresponding  $p$ -value.  $\kappa = 2$ .  $N_{\text{R}}$  is the number of runs included in the data analysis.

$\Gamma$	Stop	Start	$\alpha_{\text{fit}}$	$\sigma_{\alpha}$	$\chi_{\min}^2$	$t$	$p$	$N_{\text{R}}$
20	400	68	-1.12	0.60	1.90	0.20	0.42	52
20	360	68	-1.02	0.61	0.69	0.03	0.49	52
300	535	170	-1.40	0.87	3.21	0.46	0.32	31
20	360	68	-1.16	0.91	0.22	0.18	0.43	108
300	535	170	-1.20	0.47	1.26	0.42	0.34	115

FIG. 1: (Color online) Examples of the three autocorrelation functions,  $C(t)$ . These are the VACF ( $C_v$ ), the SACF ( $C_\lambda$ ), and the EACF ( $C_\lambda$ ). (The curves are shifted vertically for the clarity of the plot.) The corresponding transport coefficients (self-diffusion, shear viscosity, and thermal conductivity, respectively) are deemed to exist, if  $\int C(t)dt$  converges. Data here are from our simulation of a 2D Yukawa liquid at a low temperature,  $\Gamma = 300$ . Later, we will analyze data after the initial decaying oscillations but before a sound peak or zero crossing.

FIG. 2: (Color online) A  $\chi^2$  surface is used in our analysis method, for fitting a correlation function from the simulation to Eq. (12). For a value of the slope  $\alpha$  and intercept, we calculate the sum of square residuals to find  $\chi^2$ , and we repeat for many pairs of these values. The resulting values are plotted as contours. The best fit is the minimum of the  $\chi^2$  surface. A confidence interval (-0.30 to -1.32 for the fit parameter  $\alpha$  in this example) is found using the contour at a height of 2.3 above the minimum. Data shown here are for the SACF, with start and stop times of 13 and 114  $\omega_0^{-1}$ , respectively.  $\Gamma = 20$  and  $\kappa = 2$ .

FIG. 3: (Color online) Absolute value of the velocity autocorrelation functions of 2D Yukawa liquids at  $\kappa = 2$ . The heavy straight line indicates  $t^{-1}$  decay. The curves are shifted vertically for the clarity of the plot. “S” marks the spurious sound-peak feature from the traverse of the sound wave through the finite-size simulation box.

FIG. 4: (Color online) (a) Exponent  $\alpha$  characterizing the decay of the VACFs obtained from fitting straight lines to the linearly falling parts of the curves seen in Fig. 3(a). Data for additional values of  $\kappa$  are also shown. (b)  $\alpha$  as a function of the normalized temperature  $T' = T/T_M$  appears to be a nearly universal curve, with anomalous diffusion for  $T/T_M$  below about 5.

FIG. 5: (Color online) (a) Effect of  $\kappa$  and (b) system size (particle number  $N$ ) on the velocity autocorrelation functions of 2D Yukawa liquids. In (a) the coupling coefficient values are  $\Gamma = 100$ , 225, and 656, respectively, for  $\kappa = 1, 2$ , and 3. System size effects indicated by the sound peak  $S$  are most severe for small  $\kappa$ . The curves are shifted vertically for the clarity of the plots.

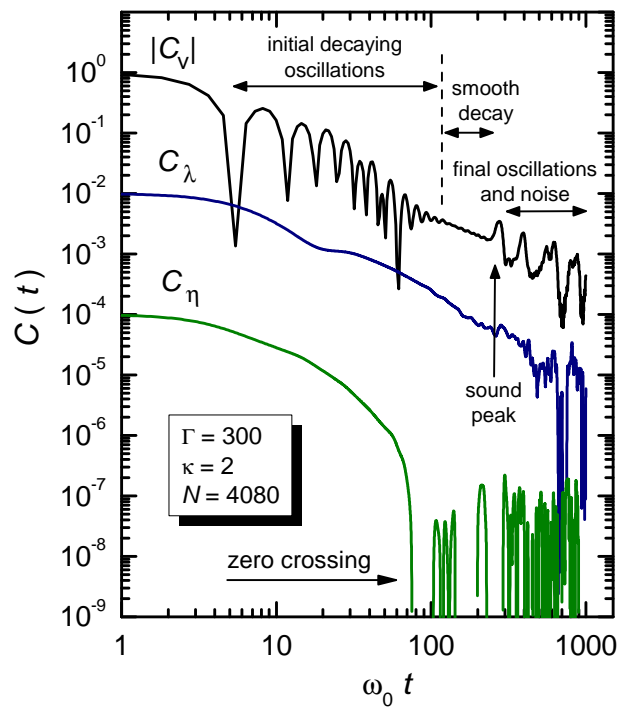
FIG. 6: (Color online) (a) Mean square displacement MSD and (b) its time derivative for different  $\Gamma$  values at  $\kappa = 2$  and  $N = 16\ 320$ . The heavy lines indicate power law behavior. The dotted vertical lines marked with “S” indicate the maximum valid time set by the sound speed.

FIG. 7: (Color online) Stress autocorrelation functions for  $\Gamma=20$  and 300,  $\kappa = 2$ . The curves are shifted vertically for the clarity of the plot. The heavy line is a power-law fit to the  $\Gamma = 20$  curve with start time =  $20\ \omega_0 t$  and stop time =  $120\ \omega_0 t$ .  $N = 16\ 320$ .

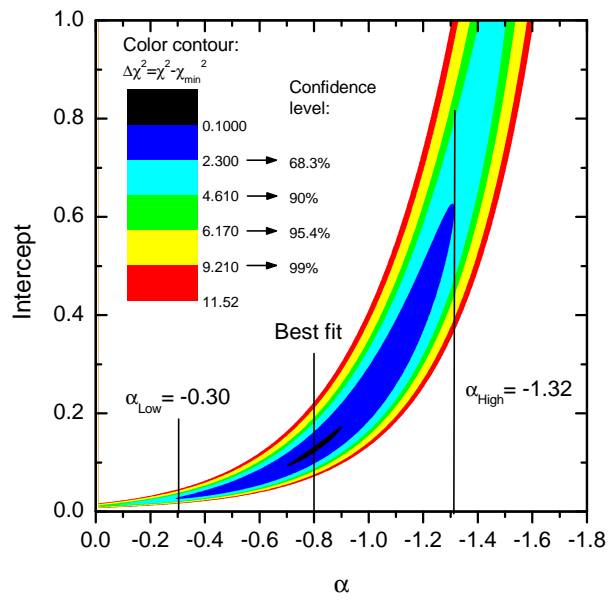
FIG. 8: (Color online) Contributions of different terms [see Eq.(10)] to the stress autocorrelation functions for (a)  $\Gamma=20$  and (b) 300,  $\kappa = 2$ .  $N = 16\ 320$ .  $C_\eta^{\text{KP}}$  is multiplied by  $-1$  in (a). Start time =  $45\ \omega_0 t$ , stop time =  $300\ \omega_0 t$  for the fit to the curve at  $\Gamma = 300$ .

FIG. 9: (Color online) Energy autocorrelation functions for  $\Gamma = 20$  and 300,  $\kappa = 2$ , and  $N = 16\ 320$ . The curves are shifted vertically for the clarity of the plot. Start time =  $68\ \omega_0 t$ , stop time =  $360\ \omega_0 t$  for the fit to the curve at  $\Gamma = 20$ .

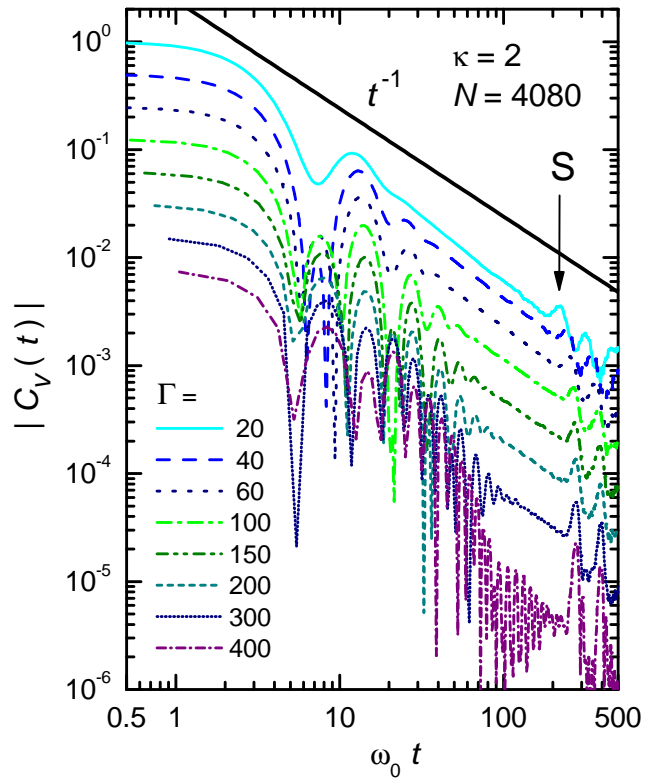
FIG. 10: (Color online) Contributions of the different terms [see Eq.(11)] to the energy autocorrelation functions for  $\Gamma = 20$  (a) and 300 (b),  $\kappa = 2$ , and  $N = 16\ 320$ .



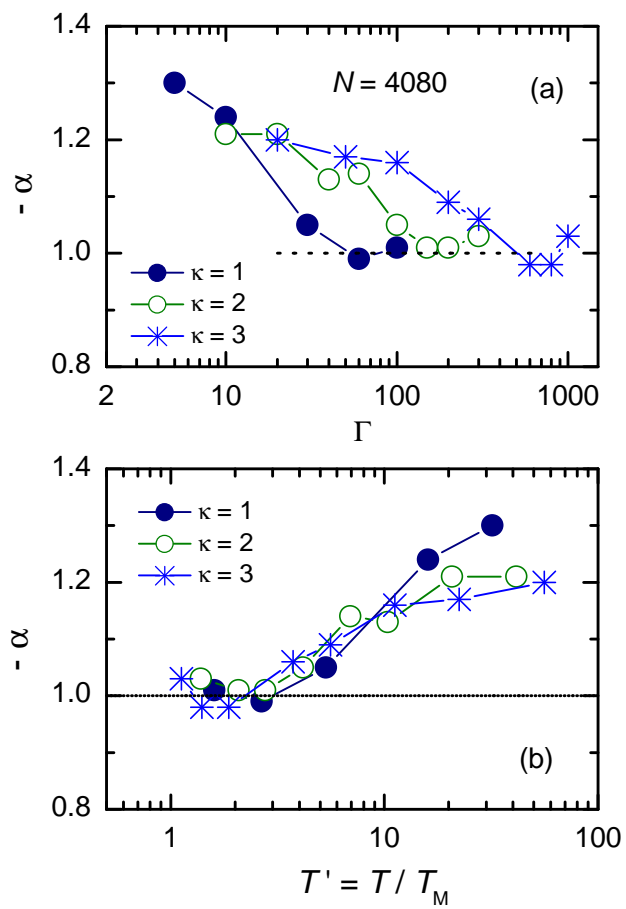
Donko, Goree, Hartmann, Liu - Figure 1.



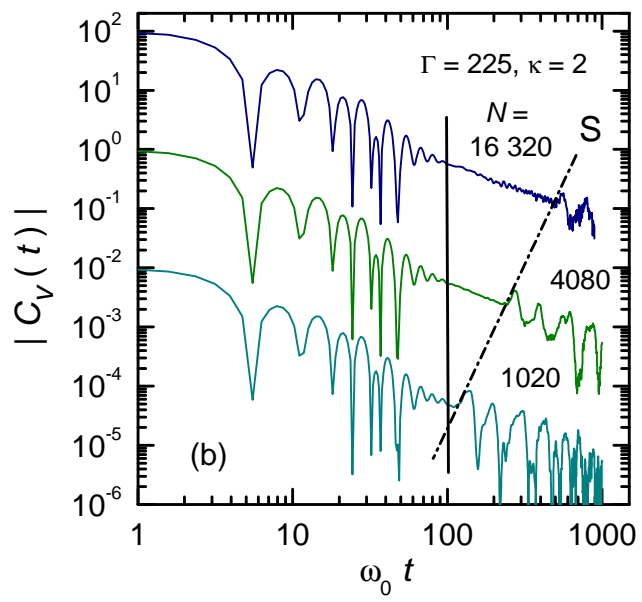
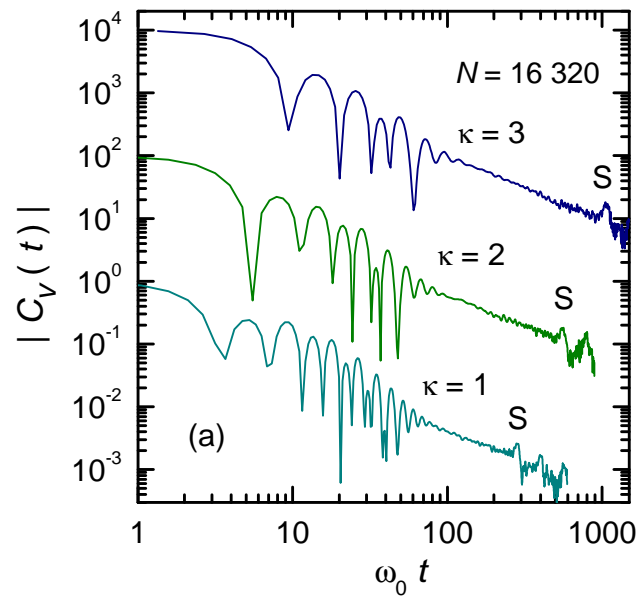
Donko, Goree, Hartmann, Liu - Figure 2.



Donko, Goree, Hartmann, Liu - Figure 3.

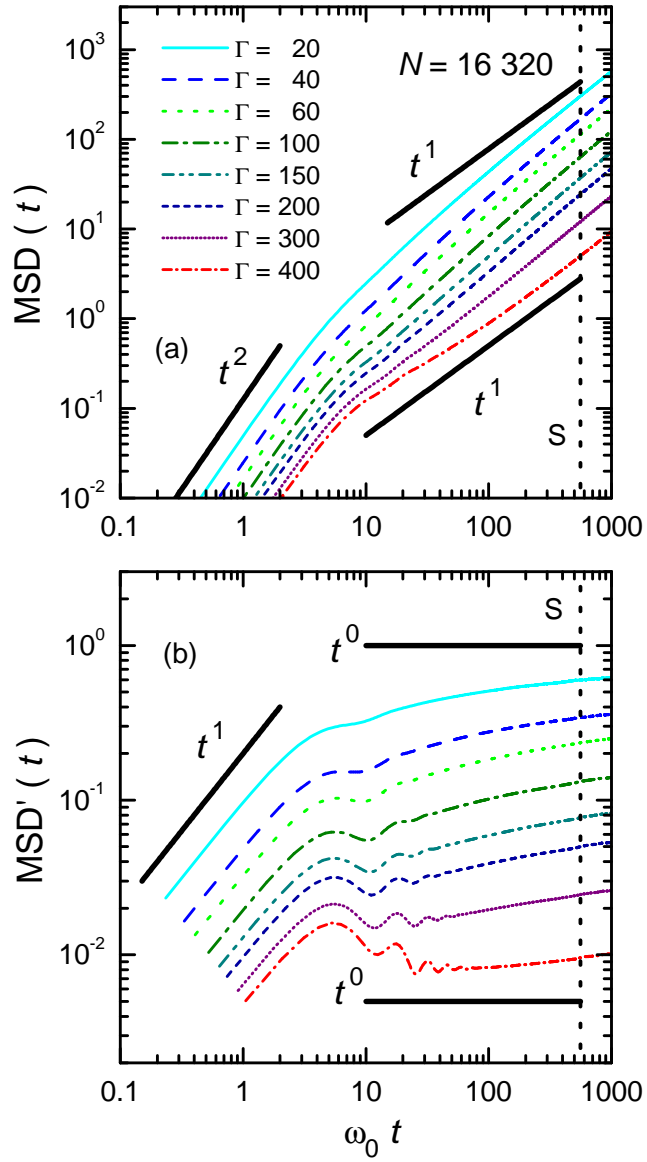


Donko, Goree, Hartmann, Liu - Figure 4.

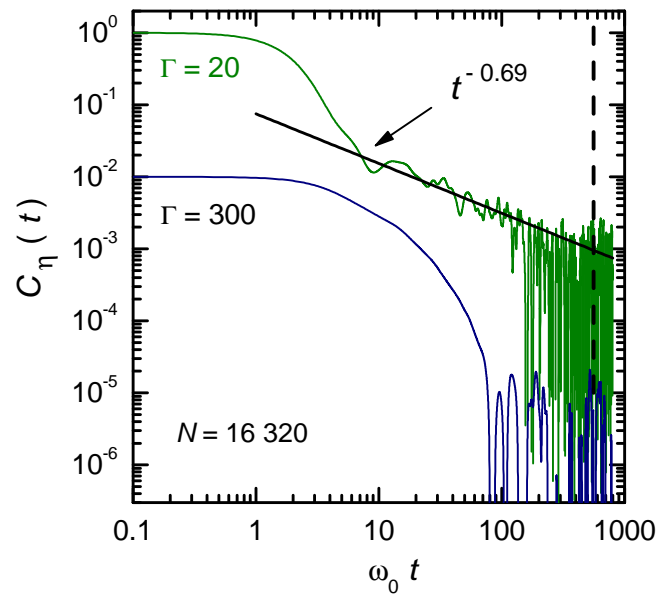


Donko, Goree, Hartmann, Liu - Figure 5.

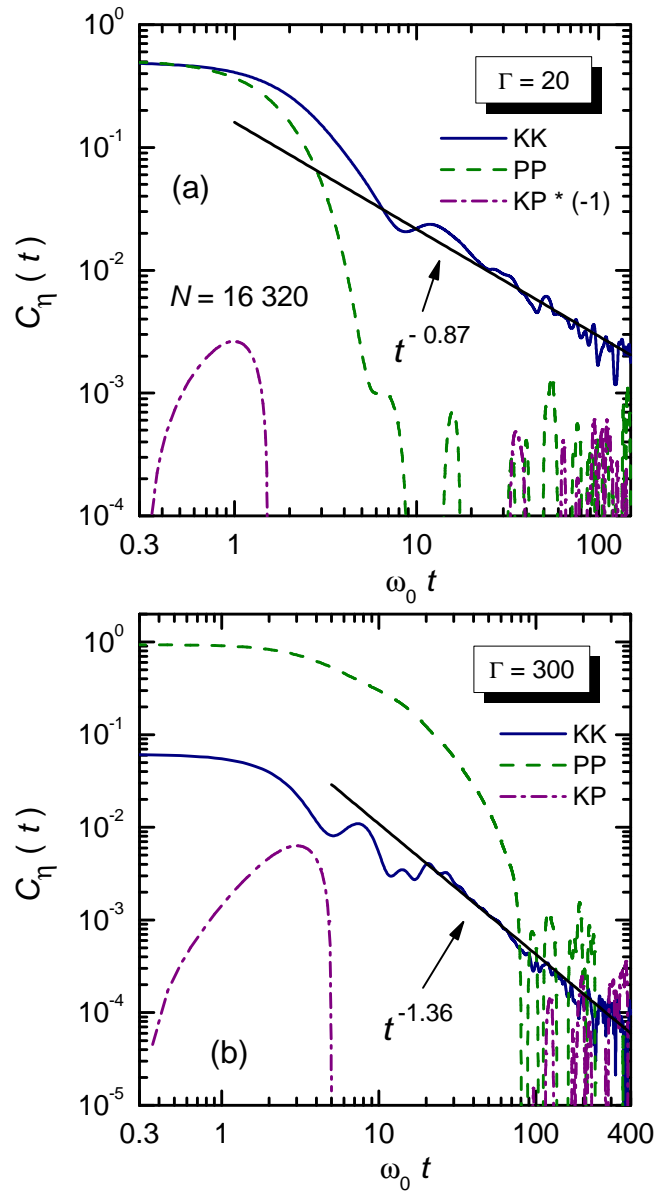




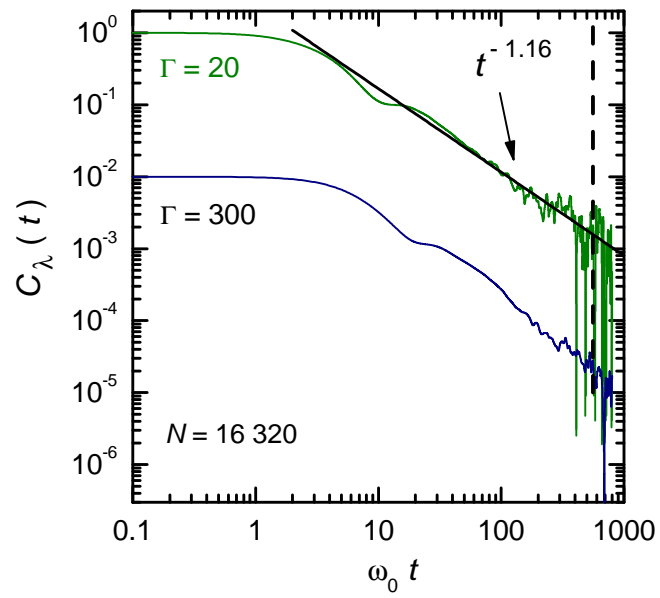
Donko, Goree, Hartmann, Liu - Figure 6.



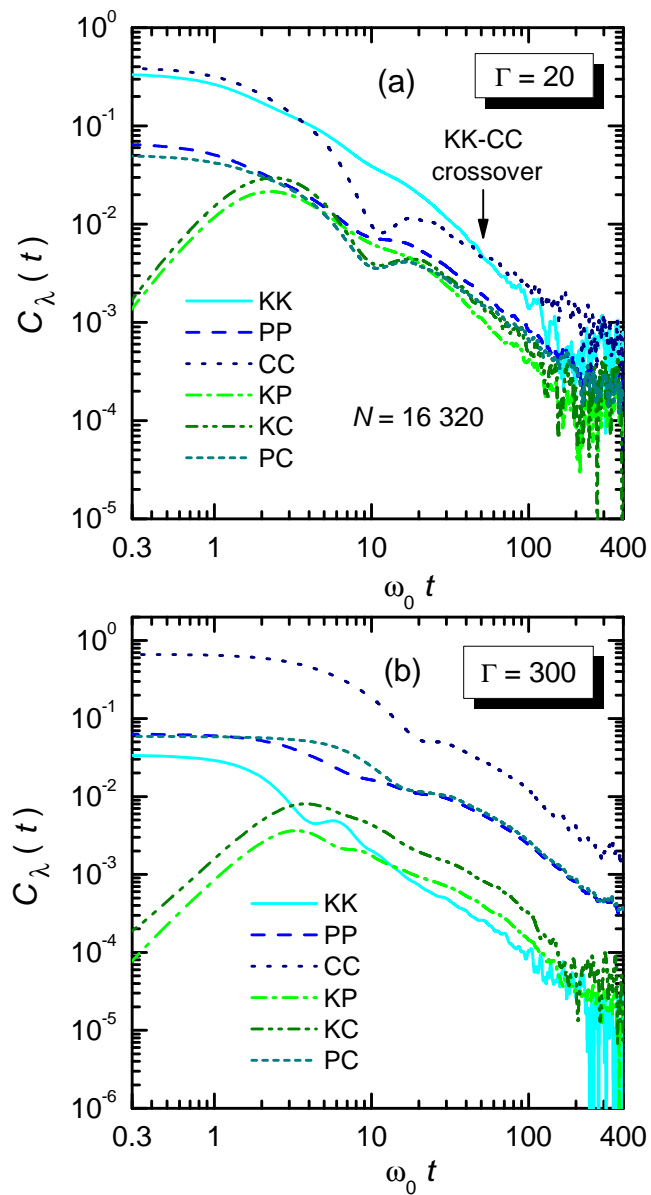
Donko, Goree, Hartmann, Liu - Figure 7.



Donko, Goree, Hartmann, Liu - Figure 8.



Donko, Goree, Hartmann, Liu - Figure 9.



Donko, Goree, Hartmann, Liu - Figure 10.